

First measurement of the Σ beam asymmetry in η photoproduction on the neutron

A. Fantini,^{1,2} R. Di Salvo,² O. Bartalini,³ V. Bellini,^{4,5} J. P. Bocquet,⁶ L. Casano,² M. Castoldi,⁷ A. D'Angelo,^{1,2} D. Franco,^{1,2} G. Gervino,^{8,9} F. Ghio,^{10,11} G. Giardina,^{12,13} B. Girolami,^{10,11} A. Giusa,^{4,13} V. Kuznetsov,^{14,15} A. Lapik,¹⁴ P. Levi Sandri,³ A. Lleres,⁶ F. Mammoliti,^{4,13} G. Mandaglio,^{12,13} M. Manganaro,^{12,13} D. Moricciani,² A. N. Mushkarenkov,¹⁴ V. Nedorezov,¹⁴ L. Nicoletti,^{2,6} C. Randieri,^{4,5} D. Rebreyend,⁶ F. Renard,⁶ N. Rudnev,¹⁴ G. Russo,^{4,13} C. Schaerf,^{1,2} M.-L. Spurduto,^{4,13} M.-C. Sutura,¹³ A. Turinge,¹⁴ and V. Vegna^{1,2}
(GRAAL Collaboration)

¹*Dipartimento di Fisica, Università degli Studi di Roma "Tor Vergata", via della Ricerca Scientifica 1, I-00133 Roma, Italy*

²*INFN-Sezione di Roma "Tor Vergata", via della Ricerca Scientifica 1, I-00133 Roma, Italy*

³*INFN-Laboratori Nazionali di Frascati, via E. Fermi 40, I-00044 Frascati, Italy*

⁴*Dipartimento di Fisica e Astronomia, Università di Catania, via Santa Sofia 64, I-95123 Catania, Italy*

⁵*INFN-Laboratori Nazionali del Sud, via di Santa Sofia 44, I-95123 Catania, Italy*

⁶*LPSC, Université Joseph Fourier Grenoble 1, CNRS/IN2P3, Institut National Polytechnique de Grenoble, 53 avenue des Martyrs, F-38026 Grenoble, France*

⁷*INFN-Sezione di Genova, via Dodecaneso 33, I-16146 Genova, Italy*

⁸*Dipartimento di Fisica Sperimentale, Università di Torino, via P. Giuria, I-00125 Torino, Italy*

⁹*INFN-Sezione di Torino, via P. Giuria, I-00125 Torino, Italy*

¹⁰*Istituto Superiore di Sanità, viale Regina Elena 299, I-00161 Roma, Italy*

¹¹*INFN-Sezione di Roma, piazzale Aldo Moro 2, I-00185 Roma, Italy*

¹²*Dipartimento di Fisica, Università di Messina, salita Sperone 31, I-98166 Messina, Italy*

¹³*INFN-Sezione di Catania, via Santa Sofia 44, I-95123 Catania, Italy*

¹⁴*Institute for Nuclear Research, RU-117312 Moscow, Russia*

¹⁵*Kyungpook National University, 1370 Sankyuk-dong, Puk-ku, Daegu, Republic of Korea*

A. Fix,¹⁶ L. Tiator,¹⁷ and S. Kamalov¹⁸

¹⁶*Laboratory of Mathematical Physics, Tomsk Polytechnic University, RU-634050 Tomsk, Russia*

¹⁷*Institut für Kernphysik, Johannes Gutenberg-Universität Mainz, D-55099 Mainz, Germany*

¹⁸*Laboratory for Theoretical Physics, JINR, Dubna, RU-141980 Moscow Region, Russia*

(Received 27 July 2007; revised manuscript received 3 March 2008; published 11 July 2008)

We present the first measurement of the Σ beam asymmetry in η photoproduction on the neutron in the photon energy range from threshold to 1.5 GeV. Data have been collected by using the tagged and linearly polarized photon beam and the large solid angle apparatus of the GRAAL facility. Neutron data have been selected among η photoproduction events on the deuteron in the quasi-free kinematics approximation. Proton data, extracted in the same way, are within errors identical to those previously obtained on free protons at the GRAAL facility, except for a few points falling in certain energy bins. This difference is, however, well understood in terms of the Fermi motion of the nucleons in the deuteron. We take the consistency of free and quasi-free proton data as an indication that nuclear effects are negligible also for neutron data. The ETAMAID model, in which a strong coupling of the $D_{15}(1675)$ resonance to the η -neutron channel is introduced, can explain the proton data very well, but it cannot describe the beam asymmetry for the neutron.

DOI: [10.1103/PhysRevC.78.015203](https://doi.org/10.1103/PhysRevC.78.015203)

PACS number(s): 25.20.Lj, 13.60.Le, 13.88.+e

I. INTRODUCTION

Pseudoscalar meson photoproduction is a powerful tool to obtain important information on baryon resonances. Among other channels η photoproduction is of special interest owing to some particular properties of ηN states: (i) the ηN system has isospin 1/2, which makes it possible to select only nucleon-like $N^*(T = 1/2)$ excitations, thus simplifying the problem of identifying individual resonances (which is not the case for pion and, especially, double pion photoproduction, where one has to deal with a large number of strongly overlapping N^* and Δ states); (ii) the background contributions in the ηN channel in the resonance region are small compared to those in pion or kaon photoproduction.

For the structure of the η photoproduction amplitude, we recall that the nucleon pole terms in s and u channels are suppressed owing to the smallness of the ηNN coupling. In contrast, an essential fraction of the background arises from ρ and ω exchange in the t -channel. But this contribution, which is important at higher energies, is almost negligible in the second and third resonance region. Therefore, η photoproduction provides a way to study baryon resonances in the absence of a strong nonresonant background.

The peculiar properties of the $\gamma N \rightarrow \eta N$ process described above have played a crucial role in the study of the $S_{11}(1535)$ (simply S_{11} from now on) resonance. Owing to its very strong coupling to the ηN channel, it has been possible to arrive

at an almost background-free identification of this state in η photoproduction. Even though the nature of the S_{11} state is still not very well understood at the fundamental level (see, e.g., Ref. [1] and references therein), recently developed phenomenological analyses [2–4] have provided interesting information about its main dynamical properties.

A number of lucky circumstances allowed these results to be obtained. First, it is known that S_{11} photoexcitation occurs in the s -wave, which makes it possible to investigate its properties without the need of using polarized photon beams and/or targets. Second, since other resonances contribute very little to η photoproduction for $E_\gamma < 0.9$ GeV, in this energy region their contribution to the total cross section is negligible.

As often remarked, this allows one to perform an accurate combined phenomenological analysis of η photoproduction on both free proton and deuteron data [5]. Indeed a simple Breit-Wigner ansatz has enabled the fitting of the energy dependence of the measured total cross sections and the extraction of an important parameter characterizing η -nucleon physics, namely the isoscalar amplitude of the S_{11} photoexcitation.

In this energy region, the polarization observables and the S_{11} dominance are expected to be of special importance. In fact, once the parameters of S_{11} are determined, one can use the previous analysis as a basis for a phenomenological study of other resonances in neutron photoproduction data obtained by making use of polarized beams and/or targets. This step relies on the fact that the S_{11} state can only be excited by electric dipole photons, with the consequence that its contribution to beam (Σ) and target (T) asymmetry is exactly zero. Thus any nonvanishing value of any one of these observables would be a signal of the interference of the S_{11} with resonances having $J \geq 3/2$. This is the reason why a measurement of Σ and/or T in η photoproduction may be a very important source of information about other resonances, which in many instances is more effective than what can be obtained from the corresponding reactions with pions.

So far no systematic experimental investigation of η photoproduction on the neutron has been performed. To study this process above the S_{11} region, where other resonances start to come into play, one must use not only inclusive η -photoproduction on the deuteron but also quasi-free processes with simultaneous measurements of the η and recoil neutron.

Besides the obvious general importance of studying neutron data, specific questions typical of η photoproduction arise here. The main problem is to understand the mechanism responsible (i) for the anomalous peak observed in the invariant mass spectrum of the η -neutron system around the value 1.65 GeV [6,7], (ii) for the larger yield of the neutron with respect to the proton for energies above the S_{11} resonance [6,7], and consequently (iii) for the nontrivial behavior of the ratio of the neutron to proton cross section observed in the region above $E_\gamma = 0.9$ GeV (see, e.g., Ref. [8] and references therein). In some recent papers, attempts were made to explain this phenomenon. For instance, in Ref. [8] two different scenarios of $\gamma n \rightarrow \eta n$ were considered: (i) a strong $D_{15}(1675)$ contribution provided by the enhanced value of $D_{15} \rightarrow \eta N$ decay width and (ii) the inclusion of an exotic narrow P_{11} resonance, as a member of a hypothetical pentaquark

antidecuplet, whose existence has been repeatedly hinted at in the literature over the past four years [6,7,9,10]. As shown in the paper [8], both models provide a qualitative description of the total cross section but predict different angular dependence, in particular of polarization observables. A third explanation for the enhancement of the neutron cross section has recently been given in terms of coupled-channel effects owing to the $S_{11}(1650)$ and $P_{11}(1710)$ resonance excitations [11]. In this alternative explanation a large pion coupling to the S_{11} resonance, accompanied by a substantial η coupling to the P_{11} , gives an enhancement in the neutron channel. We stress again that different reaction mechanisms produce different partial waves. Thus models can be distinguished from their predictions of angular distributions and polarization observables.

For the database presently available concerning η photoproduction on free protons, since the mid 1990s new target asymmetry data have been obtained at MAMI and ELSA for laboratory photon energies smaller than about 1 GeV [12,13]. Later, measurements of beam asymmetries and cross sections have been extended to higher energies at GRAAL [14–16], at JLab (where only cross sections have been measured) [17], and more recently at CB-ELSA [18]. The quality of the data has increased with time, but we are still far from having systematic polarization results covering a sufficiently wide region of energy and angle, such as the one needed as an input for a reliable multipole analysis of $\gamma N \rightarrow \eta N$ amplitudes.

In this paper we present the first systematic measurements of the Σ beam asymmetry in η photoproduction on quasi-free nucleons using the deuteron as a target. The main emphasis of the present investigation is on neutron data. The quasi-free events are identified by comparing the kinematics of the final ηN state with that of the free nucleon process.

Separate sets of data had been collected on free protons in hydrogen in identical experimental conditions and with the same apparatus. Comparison between the results obtained on free [16] and bound protons gives information about the importance of binding effects. This information is necessary to be able to correctly interpret neutron results with minimum ambiguity.

The paper is organized as follows. In the next two sections we describe the experimental setup and the method used to select the events and to extract the beam asymmetry. In Sec. IV we present the theoretical framework we use to describe η photoproduction results and we detail its application to our neutron data. Conclusions and a summary of our results can be found in Sec. V.

II. GRAAL APPARATUS AND DATA TAKING

The GRAAL facility consists of a highly polarized photon beam, produced by the Compton backscattering of laser light against the electrons of the ESRF storage ring (Grenoble, France) [19], complemented by the large solid angle apparatus LA γ RANGE (see Fig. 1 and Ref. [20] for a detailed description of both the apparatus and the γ -beam features). The laser light is almost 100% linearly polarized and the polarization of the scattered photons with the maximum allowed energy, $E_{\gamma,\max}$, is very close to that of the laser light. For photons

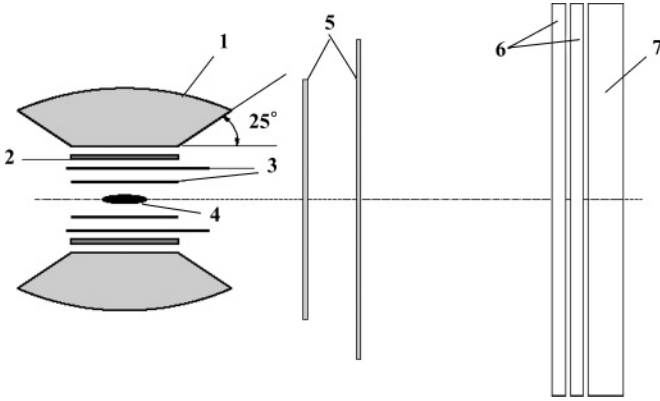


FIG. 1. Schematic view (not to scale) of the LA γ RANGE detector: (1) BGO calorimeter, (2) plastic scintillator barrel, (3) cylindrical multiwire proportional counters (MWPCs), (4) target, (5) plane MWPCs, (6) double plastic scintillator hodoscope, and (7) shower detector.

with lower energy, E_γ , a QED computation [21] shows that their polarization degree decreases as a function of the ratio $E_\gamma/E_{\gamma,\max}$.

A rotation of the beam polarization can be easily obtained by changing the direction of the laser light polarization vector by means of a half-wavelength plate. Through the use of green or multiple UV laser lines, two overlapping energy regions, from 500 to 1100 MeV and from 650 to 1500 MeV, respectively, can be covered with different polarization degrees. The agreement between results from these two independent sets of data represents a good cross-check of the stability of the GRAAL equipment and of our knowledge of the beam polarization degree.

The energy E_γ is determined by measuring, in the tagging detector, the deviation of the scattered electrons from the main orbit. The tagging detector is made of plastic scintillators, capable of providing a fast trigger of the experiment, and a silicon μ -strip position detector (128 strips), with a spatial resolution of 300 μm , which is good enough not to spoil the 16-MeV energy resolution provided by the optics of the storage ring.

The LA γ RANGE detector is composed of two parts covering distinct angular domains. At laboratory polar angles between 25° and 155° , the apparatus consists of an electromagnetic BGO calorimeter [22–24], providing a high energy resolution for γ rays [$\simeq 3\%$ (FWHM) at 1 GeV], a good response to protons with energies up to 400 MeV, and a high efficiency detection for neutrons ($\simeq 60\%$ with an energy threshold of about 2 MeV in each BGO crystal [25]). The BGO provides an angular resolution of the order of 6° – 8° (FWHM). Inside the BGO a cylindrical barrel of plastic scintillators provides ΔE measurement for charged-to-neutral particle discrimination and proton identification. Two cylindrical MWPCs for charged particle tracking [26] are located between the barrel and the target.

At laboratory polar angles $\theta < 25^\circ$ the apparatus includes 1. two planar MWPCs for charged particle tracking; 2. a double layer scintillator hodoscope, providing X, Y coordinates, ΔE , and time of flight (TOF) measurement for charged particle

identification and energy measurement for protons; and 3. a shower detector [27], yielding X, Y coordinates and TOF measurement. Neutrons and photons are detected in the shower wall with efficiencies of $\simeq 22\%$ and $\simeq 95\%$, respectively, and they are discriminated by TOF measurements, which are also used to determine the energy of protons and neutrons.

The beam flux is measured by using two detectors (beam monitors). The first one is made of three scintillators separated by a γ converter. It has a low efficiency ($\simeq 2.5\%$ – 3%) and can work at high intensities. The second one is a lead/scintillating fiber calorimeter, which also acts as a beam dump. It has 100% efficiency and it is used at low intensities [28] to calibrate the efficiency of the first one.

Asymmetries for free protons and bound protons and neutrons are extracted in similar experimental conditions, by using a 6-cm target filled with liquid hydrogen or deuterium, respectively.

The experimental trigger and the trigger for flux measurements are both provided by a signal in the tagging detector in coincidence with a signal in the BGO calorimeter (at least 180-MeV energy released in the detector) and in the beam monitors, respectively.

Data have been collected in several periods with green and multi-UV laser lines and with typical intensities of the order of $10^6 \sim \gamma/\text{s}$, integrated over the whole tagged energy spectrum. The total number of collected η mesons was around 850,000 on the proton and 290,000 on the neutron.

III. DATA ANALYSIS

A. Event selection

Events are selected according to the “participant-spectator” scheme, which assumes that the incoming photon interacts only with the “participant” nucleon, whereas the other acts as a “spectator.” Processes are then treated as two-body reactions, as if the target nucleon was free. Events will be then classified according to the reactions

$$\gamma p(n) \rightarrow \eta p(n), \quad (1)$$

$$\gamma n(p) \rightarrow \eta n(p). \quad (2)$$

Events are preselected by requiring the detection of two photons from the η decay in the BGO calorimeter, the presence of a proton or a neutron in the central or in the forward detectors, and no other particle in the apparatus. Furthermore, it is required that the two-photon invariant mass falls in the window 0.35–0.7 GeV. This window is large enough to allow a clear observation and study of the background contribution to the processes (1) and (2).

The features of the GRAAL apparatus have been simulated by employing a Monte Carlo program based on the GEANT3 code available from the CERN library. It incorporates an event generator, which produces all interesting photoproduction reactions on deuteron-bound protons and neutrons. The initial momentum assigned to the bound nucleon is extracted from a realistic Fermi distribution based on the Paris potential [29]. The simulation has been used to determine the best selection criteria and to optimize the kinematical cuts. A satisfactory agreement between the experimental and the

simulated distributions has been found for all the relevant kinematical variables.

A proton detected in the central region of the apparatus gives a signal in the three detectors (MWPC's, scintillator barrel and BGO) in geometrical coincidence, whereas a neutron gives a signal only in the BGO calorimeter. A proton detected in the forward region gives a signal either in the MWPC's, hodoscope and shower detector, or in the first two if it has a sufficiently low energy to stop in the hodoscope. The neutron can only give a signal in the shower detector.

In the energy region in which we work, protons are not relativistic, but pions are minimum ionizing particles (M.I.P.). This means that, in principle, they could be discriminated by looking at the plot of the energy lost by the particle in the scintillators as a function (a) of the energy released in the BGO (for the particles in the central detectors) or (b) of the particle TOF measured in the hodoscope (for the particles in the forward detectors). In both cases such a proton-to-pion discrimination is not possible for high-energy protons, because the two populations are not clearly separated in the plot. For this reason we decided to accept as proton candidates all charged particles and we discriminate protons from background pions only on the basis of kinematical criteria, as explained in the following.

Although neutrons in the forward direction are clearly discriminated from photons through their TOF, this is not possible in the BGO detector. The response of the BGO detector to neutrons has been simulated by using the FLUKA package [30] for hadron interactions. The simulation showed that, at the energies that are typical of this experiment, a neutron can interact in the BGO detector with only a small number of crystals. Unfortunately, low-energy photons can also produce low-multiplicity clusters and therefore a criterion based on counting the number of crystals in the cluster can only provide a first preliminary particle selection. To obtain a high photon rejection efficiency, further criteria were tried, such as the one based on the ratio between the maximum energy deposited in one crystal and the total energy of the cluster as a function of the total energy itself. As we could not find sufficiently good selection criteria, we decided to accept as possible neutron candidates all neutral particles producing low-multiplicity clusters in the BGO and we further selected the events with kinematical constraints, as we do for protons in the central and in the forward directions.

The information gathered from direct measurements in the apparatus, which we exploit in our analysis, is the following:

- (i) E_γ , the energy of the incident photon;
- (ii) E_η^{meas} , $\theta_\eta^{\text{meas}}$, and ϕ_η^{meas} , the η energy and angles; and
- (iii) θ_N^{meas} and ϕ_N^{meas} , the nucleon angles.

If a two-body kinematics is assumed, this information provides an overdetermined set of constraints. For this reason, all kinematical variables can also be calculated by using only a subset of the other measured ones. A possible choice of these calculated quantities is the following:

- (i) θ_N^{calc} , the nucleon polar angle calculated from E_γ and from the η measured energy and angles;
- (ii) E_η^{calc} , the η energy calculated from θ_N^{meas} and $\theta_\eta^{\text{meas}}$; and

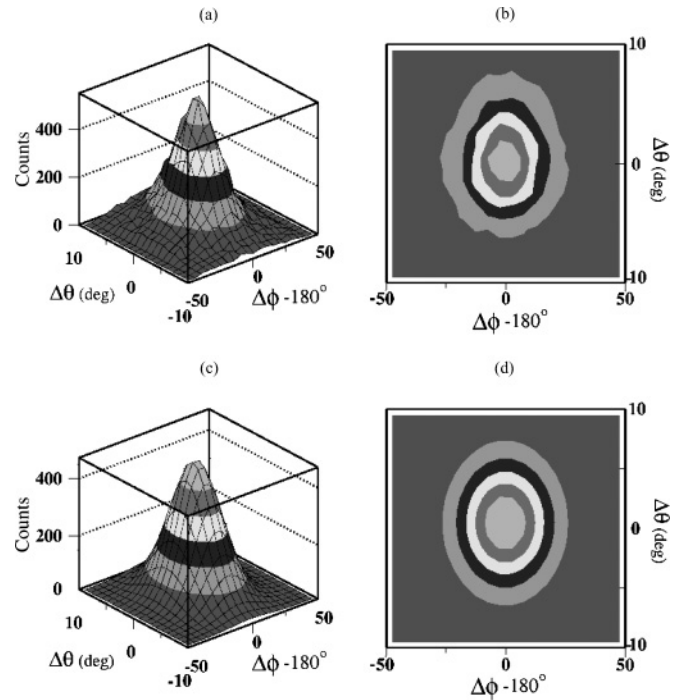


FIG. 2. (a) The correlation $\Delta\theta$ vs $\Delta\phi - 180^\circ$ in a three-dimensional view and (b) its level curve projection. (c) Bidimensional Gaussian fit and (d) its level curve projection.

- (iii) M_X , the mass of the recoil particle, calculated from E_γ and from the η measured energy and angles.

A strong background suppression is entailed by cuts in the bidimensional distributions of number of events as a function of the following two sets of complementary variables:

- (i) $\Delta\theta$, $\Delta\phi - 180^\circ$, where $\Delta\theta = \theta_N^{\text{meas}} - \theta_N^{\text{calc}}$ and $\Delta\phi = \phi_N^{\text{meas}} - \phi_\eta^{\text{meas}}$;
- (ii) $E_\eta^{\text{calc}}/E_\eta^{\text{meas}}$, $M_X - M_N$, where M_N is the nominal mass of the participant nucleon.

In Figs. 2 and 3, two examples of such event distributions are reported in a three-dimensional plot [Figs. 2(a) and 3(a)] and in a level curve projection [Figs. 2(b) and 3(b)].

The distributions of both experimental and simulated data are fitted by bidimensional Gaussians. For each distribution

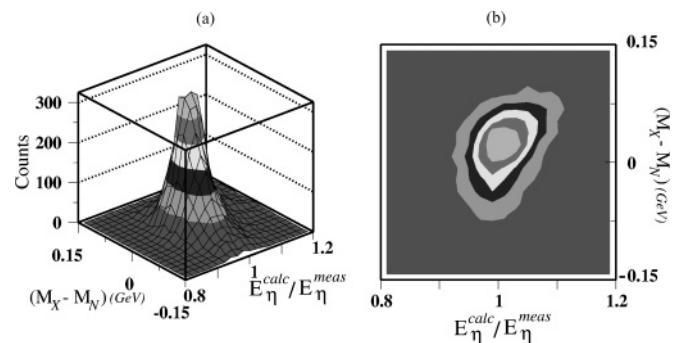


FIG. 3. (a) The correlation $E_\eta^{\text{calc}}/E_\eta^{\text{meas}}$ vs $M_X - M_N$ in a three-dimensional view. (b) Level curve projection.

we extract the values of the means, μ_x and μ_y , and widths, σ_x and σ_y , associated with the two variables on which each distribution depends. The cut applied on the two variables x, y ($\Delta\theta, \Delta\phi - 180^\circ$ or $E_\eta^{\text{calc}}/E_\eta^{\text{meas}}, M_X - M_N$) selects the events according to the condition

$$\frac{(x - \mu_x)^2}{\sigma_x^2} + \frac{(y - \mu_y)^2}{\sigma_y^2} - \frac{2C(x - \mu_x)(y - \mu_y)}{\sigma_x\sigma_y} < \sigma^2, \quad (3)$$

where $\sigma = 3$ and C is the correlation parameter.

The results from the fits of the experimental distributions are in good agreement with those from the simulated data, and for this reason we choose to extract the Gaussian parameters directly from data. In the lower part of Fig. 2 we show the fit of the distribution of the data reported in the upper part of the same figure [Fig. 2(c)] and its projection onto two dimensions [Fig. 2(d)]. For each E_γ bin a set of $\mu_{x,y}$, $\sigma_{x,y}$, and C parameters was extracted and these values have been used in setting the cuts indicated in Eq. (3).

The values of the correlation parameter C of the first cut range from a minimum of 7×10^{-3} to a maximum of 2×10^{-2} in the different energy bins. The errors on C are of the order of 2×10^{-2} or less. These values are compatible with the assumption of noncorrelated variables. For the second cut, practically all the values are around 0.5. This is because the two variables are strongly correlated, since they are derived from a common subset of measured quantities. Also in this case the errors on C are of the order of 2×10^{-2} or less.

In Fig. 4 the η invariant mass distribution is shown for a proton [Fig. 4(a)] and a neutron [Fig. 4(b)] in the central detectors and for a proton [Fig. 4(c)] and a neutron [Fig. 4(d)] in the forward detectors. In each figure the solid line represents the preselected events without kinematical cuts and the dotted line the events after the cuts. It is clear from Fig. 4(b) that even the most noisy reaction (neutron in the central region) is strongly cleaned up by the applied kinematical cuts. A more stringent cut in the η invariant mass, between 0.45 and 0.65 GeV, can be applied at this point.

From the simulation of all possible photoreactions on deuteron-bound nucleons, we verified that the use of a two-body kinematics on nucleon and η candidates rejects not only the background events coming from other competing channels, such as single or double pion photoproduction, but also not sufficiently clean events where an η and a nucleon have been detected. From our simulations we have found that the following classes of events are rejected by our selection criteria: 1. η - N events for which the Fermi momentum of the participant nucleon is too high or the spectator nucleon undergoes final-state interactions (FSIs) with the η or the participant nucleon (thus distorting the two-body kinematics); 2. η photoproduction on both nucleons, which involves three bodies in the final state; 3. η - N events for which the participant nucleon or the η was not correctly reconstructed in the apparatus; and 4. η - p (or η - n) events that have been erroneously reconstructed as η - n (or η - p) reactions, because of some inefficiency in the apparatus operation. This last class of events represents the most dangerous background, which would be particularly difficult to reject with the traditional techniques of background subtraction, since the two-photon

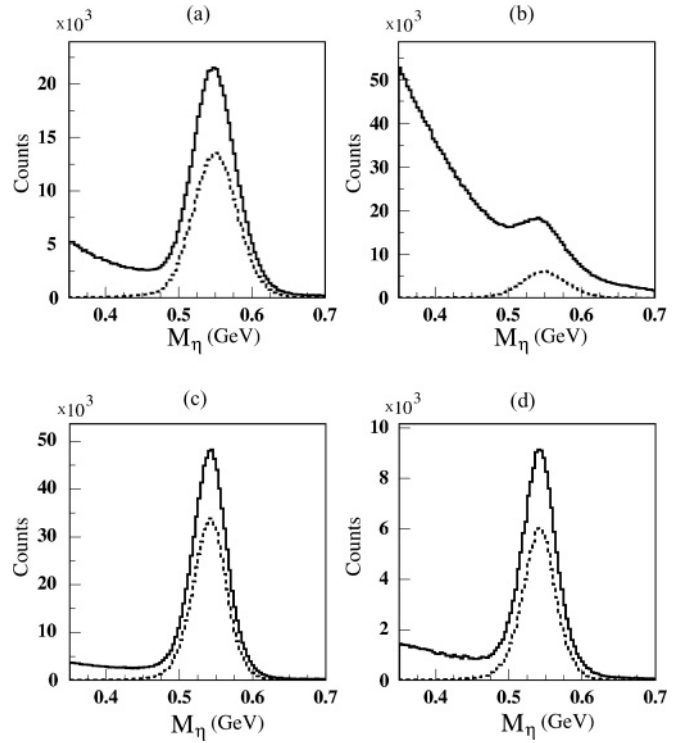


FIG. 4. The η invariant mass without cuts (solid line) and with the kinematical cuts (dotted line) for (a) a proton and (b) a neutron in the central region and for (c) a proton and (d) a neutron in the forward direction.

invariant mass spectrum shows a peak around the η mass. The use of the two-body kinematical cuts reduces it to a small percentage of the total signal. We estimated the percentage of η - p events contaminating the neutron data by evaluating the number of η - n events obtained from the analysis of data collected on a hydrogen target (where obviously only η - p reactions can take place). For neutrons in the forward direction contamination from these events is less than 0.4% and 1.8% for neutrons in the central region. Percentages of this kind are compatible with those obtained with the simulation of η photoproduction on the deuteron, which yields 0.3% for neutrons in the forward direction and 1.6% for neutrons in the central region. This last type of contamination mainly comes from the angular region where the central detector joins the forward one (i.e., in the region $\theta = 25^\circ - 30^\circ$), where a proton can be missed by both detectors. For proton reactions, this background contribution can be estimated only from simulations, yielding 0.2% for protons in the forward direction and 0.8% for protons in the central region.

The contribution of the remaining background events was estimated from the available data, by fitting the η invariant mass of the selected events with a Gaussian plus a second-degree polynomial function. In this way one finds for the background the following estimates: 1.0% for neutrons in the forward direction, 2.1% for neutrons in the central region, 0.7% for protons in the forward direction, and 1.6% for protons in the central region. These values also include the background from the target walls, which is not associated with the photoproduction of an η . Empty target data, after

kinematical cuts, have shown the presence of some η , whose number is compatible with the density of the residual gas in the target at the temperature of 25 K, plus a negligible non- η background.

Apart from the mentioned apparatus inefficiency, there are also dynamical mechanisms that may affect our selection procedure. First, the kinematic separation between spectator and participant nucleons fails when the nucleon momenta allowed in the reaction are comparable with characteristic momenta inside the deuteron. Second, the FSI results in energy and/or charge exchange between the particles, thus leading to the situation in which the spectator may eventually be interpreted as the participant nucleon. Such events are important when the limited phase space permits only low relative momenta between the final nucleons. According to the results of Refs. [31,32], in the case of η photoproduction, it is the energy region 50–70 MeV above threshold. Since our data relate to much higher energies, we neglect these effects in the present analysis.

In conclusion the total estimated background is 1.4% for neutrons in the forward direction, 3.9% for neutrons in the central region, 0.9% for protons in the forward direction, and 2.4% for protons in the central region.

B. Extracting the beam asymmetry

Selected events have been grouped together in bins with fixed values of E_γ , $\theta_\eta^{\text{c.m.}}$, and ϕ_η (where, we recall, E_γ is the γ energy and $\theta_\eta^{\text{c.m.}}$ and ϕ_η are the η polar and azimuthal angles in the c.m. system, respectively). We then define $N_{V,H}(E_\gamma, \theta_\eta^{\text{c.m.}}, \phi_\eta)$ and $F_{V,H}(E_\gamma)$ as the number of selected events and the beam flux, respectively, for vertical (V) and horizontal (H) beam polarization. The beam asymmetry, $\Sigma(E_\gamma, \theta_\eta^{\text{c.m.}})$, has been extracted by fitting the azimuthal behavior of the ratio

$$\frac{N_V/F_V}{N_V/F_V + N_H/F_H} = \frac{1}{2}[1 + P \Sigma \cos(2\phi_\eta)], \quad (4)$$

where $P(E_\gamma)$ is the beam polarization at the energy E_γ , as calculated from QED.

The detection efficiency cancels out in the ratio between the two polarization states, so that the extraction of the asymmetry is free from systematic errors from the determination of the absolute efficiency. The azimuthal distribution [Eq. (4)] has been fitted for each bin of E_γ and $\theta_\eta^{\text{c.m.}}$, as is shown in Fig. 5 for the proton (left panel) and the neutron (right panel), respectively. From the fit the product $P\Sigma$ is obtained, and from it Σ is computed from the knowledge of $P(E_\gamma)$.

The values of the asymmetry extracted in this way have been corrected for the bias introduced by the finiteness of the number of ϕ_η bins, by writing

$$\Sigma_{\text{corr}} = \Sigma(1 + R_{\phi_\eta}),$$

where the correction factor is $R_{\phi_\eta} = 2.6\%$ if the ϕ_η interval is divided into 16 bins and $R_{\phi_\eta} = 4.7\%$ if it is divided into 12 bins.

We divided the whole set of selected events into 7 energy bins for the green laser line data and 11 for the multi-UV laser

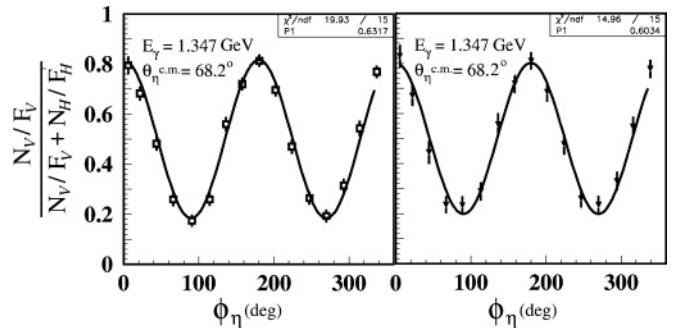


FIG. 5. The azimuthal distribution of the ratio [Eq. (4)] for the quasi-free proton (left panel) and the quasi-free neutron (right panel) data for the values of E_γ and $\theta_\eta^{\text{c.m.}}$ indicated inside the figures.

line data. We took 8 bins in the variable $\theta_\eta^{\text{c.m.}}$ and 16 in the variable ϕ_η (see Figs. 7, 9, and 10).

Separate values of the product $P\Sigma$ have been extracted for the green and the UV data, which have then been divided by the corresponding appropriate polarization value. The agreement of results obtained in overlapping energy bins confirms the reliability of our procedure. Indeed we find that the asymmetry values obtained for green and UV laser lines with different degrees of polarization are consistent with each other. In the overlapping energy region, the quoted asymmetry value in each bin is the average of the asymmetries coming from the two independent sets of data weighted according to the number of incoming photons.

Data collected with the two different laser lines have also been put together and the values of products $P\Sigma$, extracted from the fits, were divided by the mean polarization weighted on the energy spectrum of the photon beam flux corresponding to the two different laser lines. This made higher statistics available for the fits, and the asymmetry values have been extracted for $25E_\gamma$ bins, 7 bins in $\theta_\eta^{\text{c.m.}}$ and 12 in ϕ_η (Fig. 11).

We checked the stability of the asymmetry results, when the width σ of the cut [Eq. (3)] is changed from 3.0 to 2.5. The difference between the extracted asymmetry values is compatible with zero within one standard deviation in all the bins both for the neutron and for the proton. We also verified the stability of the results when we change the number of bins in ϕ_η from 12 to 16. Also in this case results are stable within one standard deviation in all bins.

To test the validity of the expression [Eq. (4)] adopted for the fit of the data, we also used a three-parameter fit, putting

$$\frac{N_V/F_V}{N_V/F_V + N_H/F_H} = A[1 + P \Sigma \cos(2\phi_\eta + B)], \quad (5)$$

where the coefficient A and the phase B are also extracted from the data: the fit [Eq. (5)] provides the values of A and B with their standard deviations; these values are compatible with 0.5 and 0, respectively, within their estimated errors for all bins. Moreover, the fitting formula [Eq. (5)] provides values of $P\Sigma$ that are compatible with the results extracted from the one-parameter fit [Eq. (4)] within their errors estimated from the fit. We checked that the χ^2 values of the one-parameter fit [Eq. (4)] are generally small and that the quality of the fits gets worse when we use a two- or three-parameter fit (with

$B = 0$); hence we concluded that the one-parameter fit is the best choice for our data.

As a further check we proceeded to extract the asymmetry of a sample of simulated events produced with a 0.5 flat asymmetry. The asymmetry values computed in this case are everywhere compatible with the simulated ones within 1–2 standard deviations.

Special attention has been paid to the calculation of the polar angle $\theta_\eta^{c.m.}$. In fact, when the Fermi momentum of the participant nucleon is composed with the momentum of the incident photon, a deviation of the Lorentz boost axis from the direction of the beam results. The angle $\theta_\eta^{c.m.}$ is calculated by taking into account this effect. The evaluation of the Fermi momentum \vec{p}_F directly from the momentum balance of the two-body reaction,

$$\vec{p}_F = \vec{p}_\eta + \vec{p}_N - \vec{p}_\gamma,$$

is affected in particular by our imprecise knowledge of the momentum of the proton (and for the neutron in the central region we have no information). For this reason we used only the best information available (i.e., the η energy and angles and the nucleon angles), whereas the energy of the outgoing nucleon, E_N^{extr} , and its momentum, p_N^{extr} , is extracted from the energy balance of the two-body reaction, with the reasonable assumption that the Fermi energy in the deuteron is negligible (since it is of the order of a few MeV). We thus write

$$E_N^{\text{extr}} = E_\gamma + M_N - E_\eta, \quad p_N^{\text{extr}} = \sqrt{(E_N^{\text{extr}})^2 - M_N^2}.$$

The extracted momentum of the outgoing nucleon is combined with its measured angles to determine its three Cartesian components $p_{N,x}^{\text{extr}}$, $p_{N,y}^{\text{extr}}$, and $p_{N,z}^{\text{extr}}$. The Fermi momentum is then calculated from the momentum balance of the two-body reaction by writing

$$\vec{p}_F = \vec{p}_\eta + \vec{p}_N^{\text{extr}} - \vec{p}_\gamma.$$

At this point the angle $\theta_\eta^{c.m.}$ is recalculated by taking into account the Fermi motion, and one obtains results well in agreement with simulations. In Fig. 6 (right panel) the distribution of the Fermi momentum is shown before and after the bidimensional cuts previously described are applied. In the left panel of Figure 6 the broadening of the coplanarity distribution owing to the Fermi motion for a bound proton (dotted line) is compared to the same distribution for a free proton (solid line).

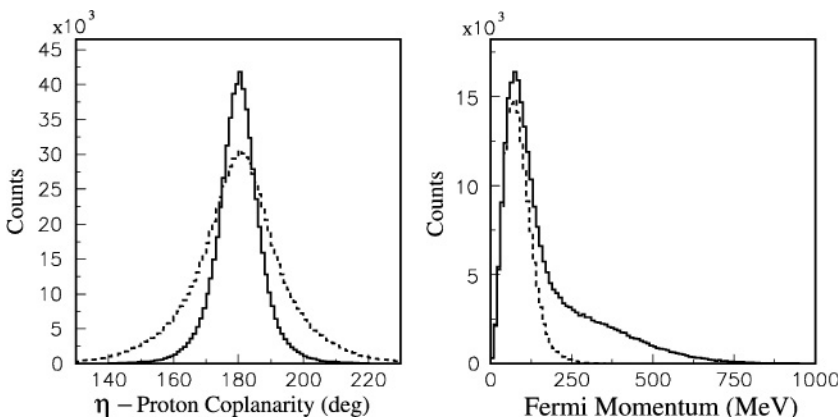


FIG. 6. (Left) Coplanarity between the η and the quasi-free proton (dotted line) and the free proton (solid line): The broadening of one distribution with respect to the other is due to the Fermi motion. (Right) The Fermi momentum distribution before (solid line) and after (dashed line) bidimensional cuts are applied (see text for details).

IV. DISCUSSION OF THE RESULTS

To compare our data with theoretical predictions we use the $\gamma d \rightarrow \eta n p$ formalism described in detail in Ref. [31] (see also Ref. [8]). It includes the familiar spectator model approximation to describe the main production mechanism with corrections from FSI (taken to first order in the ηN and $n p t$ -matrices). It is worth noting that, as the direct calculation shows [8], the FSI effects are quite small above the S_{11} resonance, so that the simple spectator model, with a realistic deuteron wave function, is expected to provide a reliable description of the reaction dynamics.

The $\gamma N \rightarrow \eta N$ amplitude is calculated by using the MAID2001 [4] as well as the reggeized MAID model [33]. A detailed description of both models can be found in the cited papers. In the MAID2001 model, the t -channel is saturated with ρ - and ω -meson exchange in the form of ordinary pole diagrams. Although this approach provides a satisfactory description up to a photon energy of about 2 GeV, it does not represent the data sufficiently well above this region. The replacement of the meson exchange diagrams with the Regge poles in Ref. [33] makes it possible to include higher spin states and thus to extend the model to higher energies on a systematic basis.

We would like to start our discussion from Fig. 7, where the results of the beam asymmetry on quasi-free protons in the deuteron are plotted (open squares) as a function of the η polar angle in the center-of-mass system, in each one of the 11 available energy bins. The error bars are statistical only. Systematic errors arise from the unsubtracted backgrounds that however (see Sec. III A) we have shown to be small. In the same figure we show for comparison the results of the beam asymmetry on free protons (full circles) obtained by the GRAAL experiment by using a hydrogen target [16]. In the same figure we plot the theoretical values of the beam asymmetry predicted by MAID2001 [4] for free proton data (dotted line) and by the two versions of MAID from Ref. [33] (dashed line) and Ref. [4] (solid line) for quasi-free protons. It is worth mentioning that, as the direct calculation shows, the difference between the solid and the dashed curve comes from the difference between the results for the free proton, found by the models of Ref. [4] and Ref. [33] which predict similar but not identical asymmetries.

At lower energies the beam asymmetry exhibits a trivial $\sin^2 \theta$ dependence (where, for shortness, θ is the η polar angle

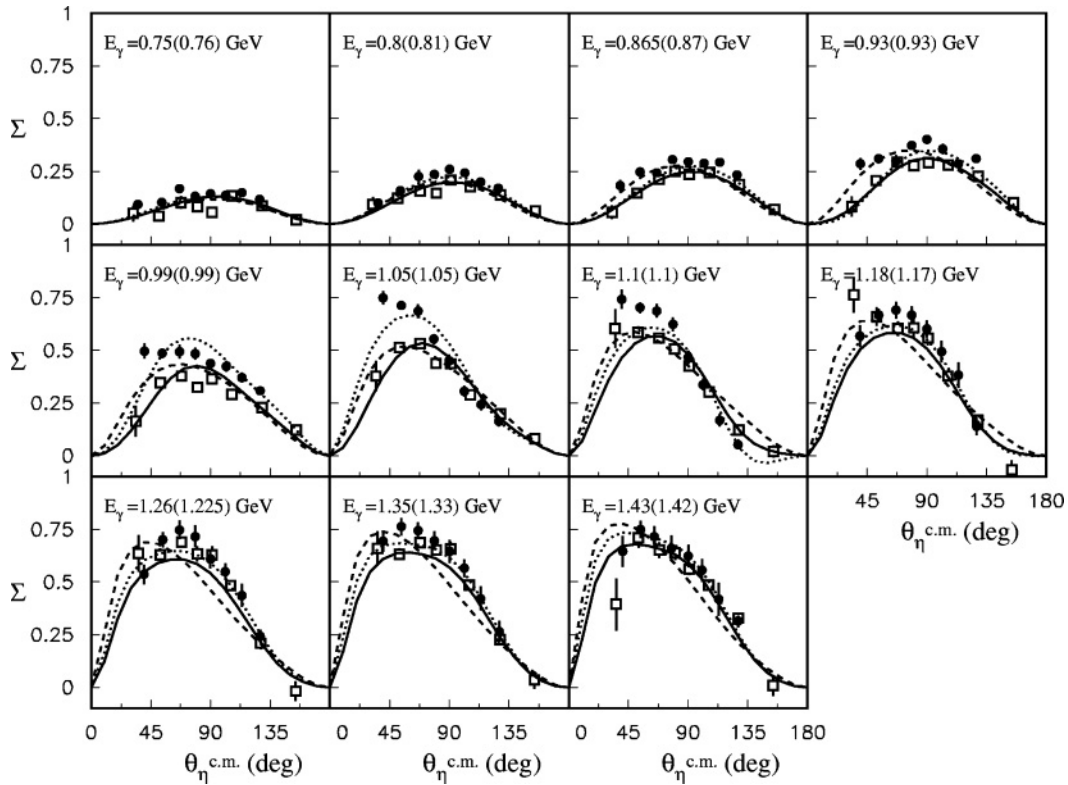


FIG. 7. Beam asymmetry Σ in η photoproduction on quasi-free protons (open squares) in the deuteron and on free protons (full circles) [16]. The energy values outside and inside parentheses indicate the mean value of the bin for quasi-free and free protons, respectively. Dotted lines are the predictions of MAID2001 [4] for the free proton; solid and dashed lines are for the quasi-free proton given by MAID2001 [4] and the reggeized model [33], respectively (see text for details).

in the c.m. system). Different analyses [3,5,34] show that in the low-energy region the process is governed by the dominance of the S_{11} resonance (contributing to the E_{0+} multipole) with a rather small admixture of other resonances, the strongest of which is the $D_{13}(1520)$ (contributing to the E_{2-} and M_{2-} multipoles). The smallness of the D_{13} contribution compared to that of S_{11} allows us to write the beam asymmetry only in terms of contributions proportional to the E_{0+} multipole according to the formula

$$\Sigma \frac{d\sigma}{d\Omega} = -3 \frac{q}{k} \sin^2 \theta \mathcal{R}e[E_{0+}^*(E_{2-} + M_{2-})]. \quad (6)$$

Since both S_{11} and D_{13} carry the same (negative) parity, the resulting Σ asymmetry is an even function of $\cos \theta$. With increasing energy, $E_\gamma > 1$ GeV, the contribution of the $L = 3$ $F_{15}(1670)$ state becomes more and more important. The positive parity of the $F_{15}(1670)$ is responsible for a clear forward-backward asymmetry. Since the contributions of D_{13} and especially that of the F_{15} are comparatively small with respect to the S_{11} contribution, the resulting beam asymmetry is well reproduced by only keeping terms proportional to E_{0+} , that is, by writing

$$\Sigma \frac{d\sigma}{d\Omega} = -3 \frac{q}{k} \sin^2 \theta \mathcal{R}e\{E_{0+}^*[(E_{2-} + M_{2-}) + 5 \cos \theta (M_{3-} + E_{3-})]\}, \quad (7)$$

where the last term, proportional to the difference $M_{3-} + E_{3-}$, is responsible for the shifting of the maximum to forward

angles. A small contribution to this multipole combination also comes from the Born terms. On the whole, we see that

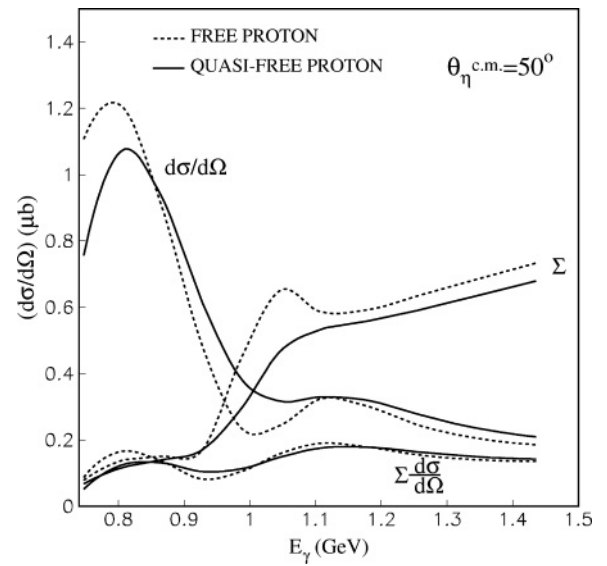


FIG. 8. Energy dependence of the differential cross section for $\gamma p \rightarrow \eta p$ calculated at $\theta_\eta^{\text{c.m.}} = 50^\circ$. The unpolarized cross section $d\sigma/d\Omega$ [Eq. (8)], the polarized cross section $\Sigma(d\sigma/d\Omega)$ [Eq. (9)], and the beam asymmetry Σ are presented. For each observable, the curves for a free proton (dashed curve) and a quasi-free proton (solid curve) are shown.

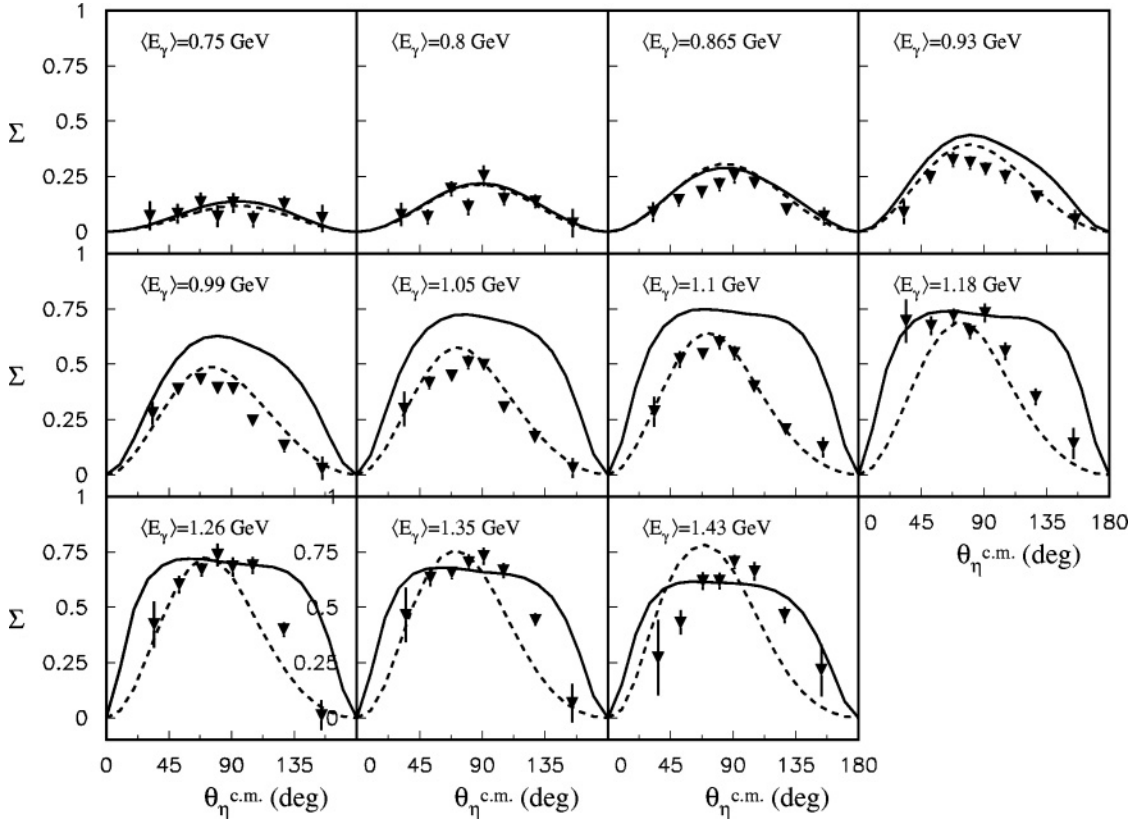


FIG. 9. Beam asymmetry Σ in η photoproduction on quasi-free neutrons in the 11 bins in which the energy range has been divided, plotted as a function of $\theta_\eta^{\text{c.m.}}$. In each plot, the mean γ energy of the bin is also indicated. Solid and dashed lines illustrate the predictions for neutrons of MAID2001 [4] and of the reggeized model [33], respectively (see text for details).

the dominant experimental features of the beam asymmetry in $\gamma p \rightarrow \eta p$ (i.e., the $\sin^2 \theta$ dependence with a slight forward-backward asymmetry at higher energies) are well reproduced by the model.

As expected, the results for the quasi-free proton are close to those obtained on the free proton. Thus the bound-nucleon effects, and in particular the Fermi motion, are of minor importance. This conclusion seems to be true in the data for almost all the energies considered, except for the region in which E_γ is around 1 GeV. A difference between the solid and the dashed curves, visible in three bins, from $E_\gamma \simeq 0.93$ GeV to $E_\gamma \simeq 1.04$ GeV, deserves a special comment. To explain the source of this effect, we present in Fig. 8 the energy dependence of the unpolarized cross section

$$\frac{d\sigma}{d\Omega} = \frac{1}{2} \frac{d\sigma_\perp + d\sigma_\parallel}{d\Omega} \quad (8)$$

for $\theta = 50^\circ$ and for the asymmetry

$$\Sigma \frac{d\sigma}{d\Omega} = \frac{1}{2} \frac{d\sigma_\perp - d\sigma_\parallel}{d\Omega}. \quad (9)$$

Here as usual σ_\perp and σ_\parallel denote the cross sections related to photons with polarization perpendicular and parallel to the reaction plane. Of crucial importance is the minimum seen in the unpolarized cross section close to $E_\gamma \simeq 1$ GeV. When the proton is embedded into the deuteron, the Fermi motion fills

this minimum because of smearing of the resonance structure. As a result, the value of $d\sigma/d\Omega$ is increased. In contrast to the unpolarized cross section, the difference $d\sigma_\perp - d\sigma_\parallel$ undergoes only a rather small change from free to bound proton, owing to a cancellation of the S_{11} excitation. All these effects tend to reduce the value of the resulting beam asymmetry Σ (see Fig. 8). The considerations developed here show that in discussing and modeling the impact of the Fermi motion on quasi-free processes, two issues play a crucial role. One has to do with the observation that we are dealing with events taking place around threshold (where the spreading of momenta from the Fermi motion is particularly relevant) and the second is the specific behavior of the elementary differential cross sections with energy (which show a peculiar structure of maxima and minima).

We now consider the neutron channel. In Fig. 9 the first results of the Σ beam asymmetry on quasi-free neutrons in the deuteron are shown. The angular behavior is symmetric around 90° up to 0.9 GeV. Above and up to 1.25 GeV the curve shows a peak in the forward direction. Finally, in the highest energy bins its behavior looks symmetric again.

The theoretical curves shown in Fig. 9 are calculated by using the two models mentioned in the introduction: MAID2001 (solid line), where a large contribution from the $D_{15}(1675)$ resonance is introduced, and the reggeized model (dashed line), where the coupling of D_{15} to ηN is reduced down to

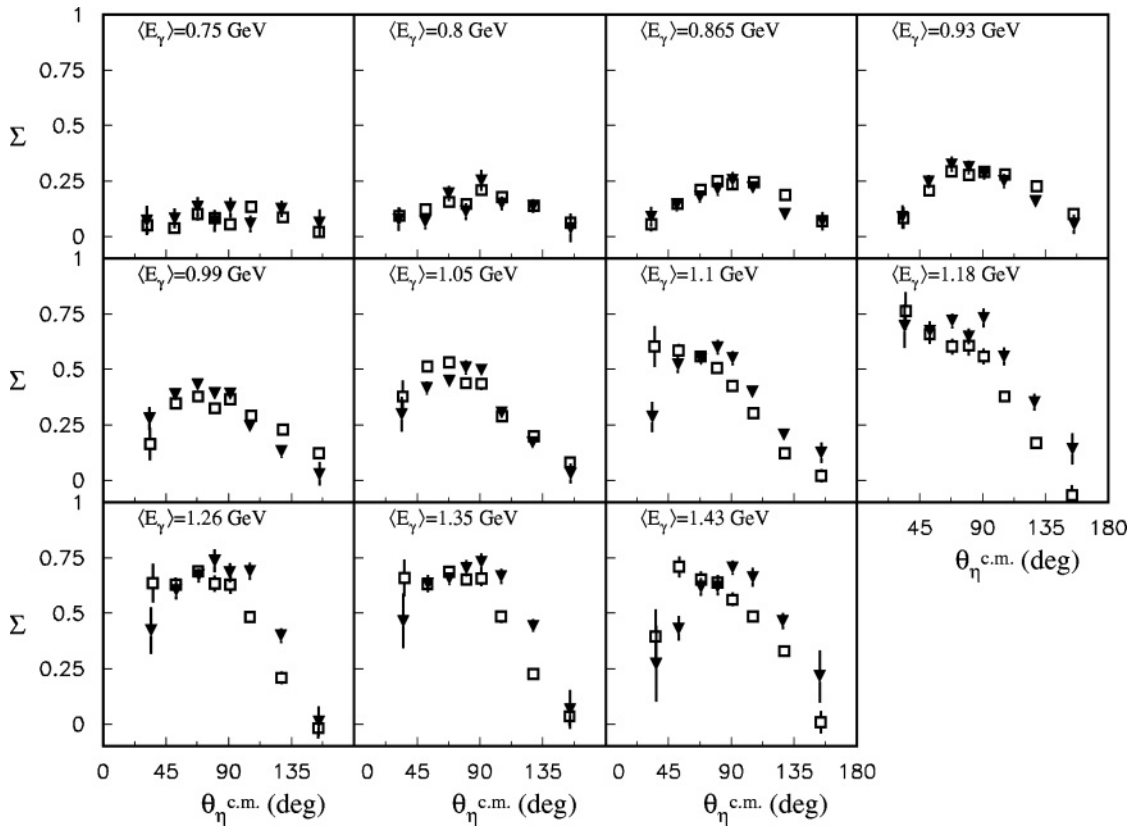


FIG. 10. Comparison between the beam asymmetry Σ in η photoproduction on quasi-free protons (open squares) and quasi-free neutrons (full triangles) in the 11 bins in which the energy range has been divided, plotted as a function of $\theta_\eta^{c.m.}$. See text for details.

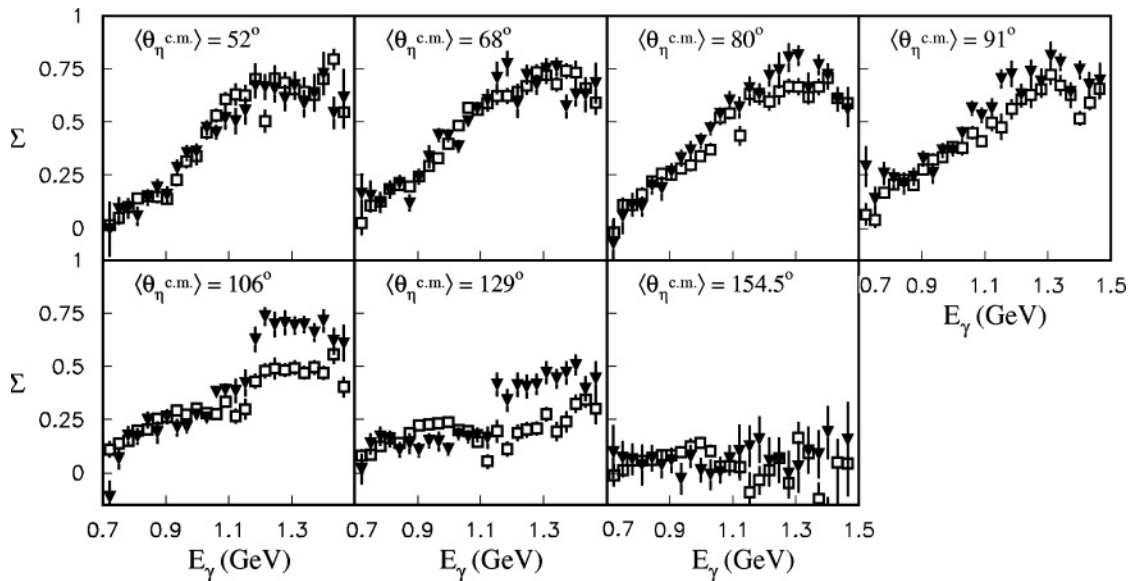


FIG. 11. Comparison between the beam asymmetry Σ in η photoproduction on quasi-free protons (open squares) and quasi-free neutrons (full triangles) in the seven bins in which the angle range has been divided, plotted as a function of the γ energy.

about 1.7%. Whereas for the free proton both models yield approximately the same energy behavior of cross section and beam asymmetry, they predict very different results in the neutron case. The reason is that the importance of the D_{15} contribution significantly increases in the neutron case, primarily because of the strong dominance of the neutron channel γn in D_{15} photodecay. The theoretical Σ asymmetry coming from taking into account the contribution of the S_{11} and D_{15} resonances is

$$\Sigma \frac{d\sigma}{d\Omega} = \frac{3}{2} \frac{q}{k} \sin^2 \theta (A + 15B \cos^2 \theta), \quad (10)$$

where the coefficients A and B are expressed in terms of the appropriate multipole amplitudes as

$$\begin{aligned} A &= \mathcal{R}e[2E_{0+}^*(E_{2+} - M_{2+}) + 3E_{2+}^*M_{2+}] \\ &\quad - 6|E_{2+}|^2 + 3|M_{2+}|^2, \\ B &= |M_{2+}|^2 - \frac{1}{2}|E_{2+}|^2 + \mathcal{R}e(E_{2+}^*M_{2+}). \end{aligned} \quad (11)$$

Furthermore, the M_{2+} multipole largely dominates over E_{2+} and Eq. (10) simplifies to

$$\begin{aligned} \Sigma \frac{d\sigma}{d\Omega} &= -3 \frac{q}{k} \left[(E_{0+}^*M_{2+} - 9|M_{2+}|^2) \sin^2 \theta \right. \\ &\quad \left. + \frac{15}{2} |M_{2+}|^2 \sin^4 \theta \right]. \end{aligned} \quad (12)$$

The last term in Eq. (12) generates a large $\sin^4 \theta$ contribution, modifying the simple $\sin^2 \theta$ behavior observed below the $D_{15}(1675)$ threshold energy. As a result of the interplay between the two terms in Eq. (12), the Σ asymmetry exhibits a plateau, as indicated by the solid curves in Fig. 9, which is however not visible in the data. As one can see, by and large, the Regge model [33] provides a better description of the beam asymmetry on the neutron. Small deviations are only seen at energies above 1.3 GeV, where there is the tendency of shifting the maximum too far into the forward hemisphere.

The comparison between the asymmetries on the proton (Σ_p) and on the neutron (Σ_n) are displayed in Fig. 10 as a function of $\theta_n^{\text{c.m.}}$ for 11 energy bins and in Fig. 11 for 7 angular bins, as a function of the γ energy in intervals of about 25 MeV. The figures show that Σ_n is quite close to Σ_p up to an energy of 1.05 GeV and starts to deviate at higher energies especially at backward angles. This could mean that the contribution of the most important mechanisms is similar in ηp and ηn channels up to 1.05 GeV. Thus the model of Ref. [33], where the most important resonances are almost equally coupled to neutron and proton, yields a better fit to our data. At the same time, as is shown in Ref. [8], the reggeized model produces a cross section that is too small with respect to the data for quasi-free η photoproduction on neutrons in the region above the S_{11} resonance [7,35] and explains neither the observed ratio of the neutron to proton cross section nor the measured differences between proton and neutron asymmetries. To solve the difficulty in fitting the cross-section and asymmetry data, the authors of Refs. [7,8] have added to the traditional isobar model a narrow resonance

$P_{11}(1670)$, which is believed to be a member of a hypothetical pentaquark multiplet $\overline{10}$. Its photocoupling is dominated by the γn mode [9], so this resonance can be safely added without spoiling any of the features of the successful $\gamma p \rightarrow \eta p$ fit. Another scenario, namely the combined effect of $S_{11}(1650)$ and $P_{11}(1710)$ resonances predicted by the Giessen model, was discussed in Ref. [11]. The prediction for Σ_n (see Fig. 9 in Ref. [11]) does not disagree with our data. The slight shift of the maximum into the forward hemisphere seen in the region $E_\gamma = 1.0$ –1.2 GeV could be due to a large contribution of the $P_{11}(1710)$ resonance. Neither of the two explanations is really satisfactory and the data pose quite a challenge to theoreticians to reveal the underlying physics. Clearly any theoretical investigation in this field should be based on a detailed analysis of the observables related to the $\gamma n \rightarrow \eta n$ process. We expect that our results will be a motivation for further studies in this field.

V. CONCLUSIONS

The GRAAL facility has provided new high-quality data on the Σ beam asymmetry in η photoproduction on protons and neutrons in the energy range from 0.7 to 1.5 GeV. Both sets of data are extracted from the quasi-free reaction $\gamma N \rightarrow \eta N$ where the deuteron is used as a target. Comparison of the results on free and quasi-free protons shows that, except for the regions where the unpolarized cross section rapidly changes, the Fermi motion only weakly influences the value of the Σ asymmetry, suggesting that also the asymmetry measured on a quasi-free neutron should be very similar to what one would measure on a hypothetical free neutron.

In general the θ dependence of Σ_n shows that, between the two models of Refs. [4] and [33], the data favor the second one, where a Regge behavior is introduced to describe vector meson exchanges. The model presented in Ref. [11] also yields a reasonable agreement with our experimental results. The measured asymmetry values in $\gamma n \rightarrow \eta n$ do not show the strong $\sin^4 \theta$ component in θ dependence predicted by the $S_{11} + D_{15}$ ansatz. The energy dependence of the Σ_n and Σ_p asymmetries is very similar up to the bin energy 1.05 GeV. At higher energies the proton asymmetries are more forward-peaked, whereas those on the neutron look more symmetric around $\theta = 90^\circ$. In particular at backward angles and energies above ~ 1.05 GeV, the neutron asymmetry values are substantially higher than those of the proton.

ACKNOWLEDGMENTS

We wish to thank all the technical staff of the collaboration teams, who gave support for the maintenance of the apparatus and of the target. We are grateful to the ESRF as a host institution for the stable operation of the electron beam and to the members of the CRG support group for the technical assistance that they provide to the GRAAL Collaboration. We wish to thank Prof. G.C. Rossi, of the University of Roma ‘‘Tor Vergata’’, for a critical reading of the preliminary draft and substantial improvements.

- [1] V. Baru *et al.*, nucl-th/0610011.
- [2] Ch. Sauermann, B. L. Friman, and W. Nörenberg, Phys. Lett. **B341**, 261 (1995).
- [3] M. Benmerrouche, N. C. Mukhopadhyay, and J. F. Zhang, Phys. Rev. D **51**, 3237 (1995).
- [4] W.-T. Chiang, S. N. Yang, L. Tiator, and D. Drechsel, Nucl. Phys. **A700**, 429 (2002).
- [5] B. Krusche *et al.*, Phys. Lett. **B358**, 40 (1995).
- [6] C. Schaerf *et al.*, Published in Tallahassee 2005, Physics of excited nucleons 176–184; V. Kuznetsov, hep-ex/0601002; R. Di Salvo, Int. J. Mod. Phys. A **20**, 1918 (2005).
- [7] V. Kuznetsov *et al.*, Phys. Lett. **B647**, 23 (2007).
- [8] A. Fix, L. Tiator, and M. V. Polyakov, Eur. Phys. J. A **32**, 311 (2007).
- [9] M. V. Polyakov and A. Rathke, Eur. Phys. J. A **18**, 691 (2003).
- [10] R. A. Arndt, Ya. I. Azimov, M. V. Polyakov, I. I. Strakovsky, and R. L. Workman, Phys. Rev. C **69**, 035208 (2004).
- [11] V. Shklyar, H. Lenske, and U. Mosel, Phys. Lett. **B650**, 172 (2007).
- [12] B. Krusche *et al.*, Phys. Rev. Lett. **74**, 3736 (1995).
- [13] A. Bock *et al.*, Phys. Rev. Lett. **81**, 534 (1998).
- [14] J. Ajaka *et al.*, Phys. Rev. Lett. **81**, 1797 (1998).
- [15] F. Renard *et al.*, Phys. Lett. **B528**, 215 (2002).
- [16] O. Bartalini *et al.*, Eur. Phys. J. A **33**, 169 (2007).
- [17] M. Dugger *et al.*, Phys. Rev. Lett. **96**, 062001 (2006).
- [18] D. Elsner *et al.*, Eur. Phys. J. A **33**, 147 (2007).
- [19] D. Babusci *et al.*, Riv. Nuovo Cimento **19**, N. 5, 1 (1996).
- [20] O. Bartalini *et al.*, Eur. Phys. J. A **26**, 399 (2006).
- [21] F. R. Arutyunian *et al.*, Sov. Phys. Usp. **7**, 339 (1964).
- [22] P. Levi Sandri *et al.*, Nucl. Instrum. Methods Phys. Res. A **370**, 396 (1996).
- [23] F. Ghio *et al.*, Nucl. Instrum. Methods Phys. Res. A **404**, 71 (1998).
- [24] M. Castoldi *et al.*, Nucl. Instrum. Methods Phys. Res. A **403**, 22 (1998).
- [25] O. Bartalini *et al.*, Nucl. Instrum. Methods Phys. Res. A **562**, 85 (2006).
- [26] A. Lleres *et al.*, Eur. Phys. J. A **31**, 79 (2007).
- [27] V. Kuznetsov *et al.*, Nucl. Instrum. Methods Phys. Res. A **487**, 396 (2002).
- [28] V. Bellini *et al.*, Nucl. Instrum. Methods Phys. Res. A **386**, 254 (1997).
- [29] M. Lacombe *et al.*, Phys. Rev. C **21**, 861 (1980).
- [30] A. Fassò *et al.*, CERN 2005-10 (2005); INFN/TC.05/11; SLAC-R-773.
- [31] A. Fix and H. Arenhövel, Z. Phys. A **359**, 427 (1997).
- [32] J. Weiss *et al.*, Eur. Phys. J. A **16**, 275 (2003).
- [33] W.-T. Chiang, S. N. Yang, L. Tiator, M. Vanderhaeghen, and D. Drechsel, Phys. Rev. C **68**, 045202 (2003).
- [34] G. Knöchlein, D. Drechsel, and L. Tiator, Z. Phys. A **352**, 327 (1995).
- [35] B. Krusche *et al.*, Eur. Phys. J. A **31**, 485 (2007).